Baroclinic Jets in Confluent Flow*

MICHAEL A. SPALL

Woods Hole Oceanographic Institution, Woods Hole, Massachusetts

(Manuscript received 21 February 1996, in final form 25 October 1996)

ABSTRACT

The nonlinear, three-dimensional behavior of baroclinic fronts in a barotropic deformation field is investigated. A major finding is that baroclinic instability of the frontal zone can play an important role in limiting frontogenesis forced by the large-scale deformation. This results in a statistically equilibrated state in which the front oscillates about a mean vertical shear and frontal width. This equilibration mechanism is effective over a wide range of parameter space and is relevant to a variety of fronts in both the ocean and the atmosphere. Sufficiently strong deformation fields, however, can stabilize the baroclinic jet, yielding the two-dimensional result in which the frontogenesis is ultimately limited by the model subgrid-scale mixing parameterization. The time-dependent three-dimensional equilibrated state is achieved for those cases in which perturbations can grow to sufficient amplitude such that the nonlinearities counteract the frontal steepening induced by the large-scale deformation field through the large amplitude baroclinic wave cycle and resulting heat flux. The regimes of the steady equilibrated state and the time-dependent equilibrated state are predicted well by an application of Bishop's linear model of time-dependent wave growth. The vertical heat flux and subduction rate are dominated by the essentially two-dimensional ageostrophic circulation resulting from the large-scale deformation field, not by the eddy heat flux associated with baroclinic instability. The ageostrophic horizontal and vertical circulations, and vertical heat flux and subduction rates, are discussed and compared to various oceanic observations.

1. Introduction

Large-scale deformation fields are often responsible for the formation, enhancement, and maintenance of fronts throughout the world's oceans and atmosphere. As discussed by Hoskins and Bretherton (1972, hereafter HB72), horizontal deformation, horizontal shear, vertical deformation, and vertical shear may form sharp gradients from initially weak gradients in both dynamically active and passive tracers. The process by which weak horizontal gradients are intensified into strong fronts is generally referred to as frontogensis. The present study addresses the three-dimensional frontogenesis of an initially weak baroclinic zone under horizontal deformation.

Large-scale deformation fields can be provided by several physical processes. In the ocean, the wind-driven Ekman transport is generally convergent in the latitude bands between the midlatitude westerlies and the tropical trade winds. These regions, referred to as subtropical convergence zones (STCZ), are regions of enhanced upper-ocean meridional density gradients in the climatological mean over spatial scales of several hundred kilometers. However, high-resolution surveys of the STCZs in both the Pacific (Roden 1980) and Atlantic (Voorhis 1969) Oceans often reveal that this climatological large-scale gradient is achieved by multiple time-dependent strong frontal bands of O(10 km) width. The spatial scales and complex patterns of these surface fronts suggest that their formation and maintenance cannot be explained by Ekman transports alone (Halliwell et al. 1991, hereafter H91; Halliwell and Cornillon 1989), although the Ekman transport is probably responsible for the larger-scale enhancement of the meridional density gradient in these regions. The geostrophic flow field can also provide horizontal deformation fields on both the gyre scale, for example, as represented by the northern and southern Gulf Stream recirculation gyres, and on the mesoscale, as provided, for example, by thermocline eddies in the STCZ of the North Atlantic (H91; Halliwell 1997, manuscript submitted to *J. Phys. Oceanogr.*, hereafter H97) and in the North Pacific (Van Woert 1982). Observations show that the transient open ocean frontal bands are often found in the mixed layer along the perimeter of these mesoscale eddies (Halliwell and Cornillon 1989; H91; Van Woert 1982; H97), suggesting that the deformation field provided by the eddies is in part responsible for the existence of the strong SST fronts. A somewhat similar

*Woods Hole Oceanographic Institution Contribution Number 9296.

Corresponding author address: Dr. Michael A. Spall, Dept. of Physical Oceanography, Woods Hole Oceanographic Institution, MS #21, 360 Woods Hole Road, Woods Hole, MA 02543.
E-mail: mspall@whoi.edu

horizontal deformation field is found in the atmosphere between adjacent cyclonic and anticyclonic circulations along a baroclinic front (HB72). The dynamics discussed in this paper are relevant to each of these frontal regions (among others), although available data in the vicinity of the STCZ fronts has prompted a more detailed look at similar fronts in the present study.

The two-dimensional formation and short time evolution of fronts in horizontal deformation fields has been extensively studied as a means to understand the intensification period and sense of the ageostrophic circulation in the vicinity of fronts in both the atmosphere (e.g., Sawyer 1956; HB72; Williams 1974; Gall et al. 1987; Snyder et al. 1993) and the ocean (MacVean and Woods 1980; Bleck et al. 1988, hereafter BOW88; Rudnick and Davis 1988). If one invokes conservation of potential vorticity, it can be shown that there will be downwelling on the cold side of the front and upwelling on the warm side of the front with an ageostrophic cross-front flow from the warm side to the cold side near the boundary (HB72; BOW88). The analytic solution to the semigeostrophic equations predicts a discontinuity at the boundary in a finite time (HB72). Models of the intensification phase of frontogenesis generally either 1) do not extend in time far enough to reach the discontinuity (HB72); 2) invoke some form of unresolved turbulent mixing to balance the heat convergence at the boundary (Williams 1974; Gall et al. 1987); or 3) limit the amount of potential energy available to the developing front (BOW88). Observations are generally consistent with these two-dimensional models in terms of the frontal formation and sense of the ageostrophic circulation. However, most observed fronts do not collapse to extremely small scales and are generally limited to relative vorticities on the order of the planetary vorticity. This implies the existence of some process acting on these horizontal scales that counteracts the frontogenesis. The large amplitude, three-dimensional regime has not yet been explored in detail and, in particular, the question of what ultimately balances the frontal collapse in horizontal deformation fields has remained largely unanswered.

Fronts often exhibit time-dependent meandering, sometimes growing to sufficient amplitude such that discrete vortices are formed. Numerical models have often been used to study the large amplitude behavior of baroclinic wave growth and vortex formation by oceanic fronts in the absence of any external frontogenesis mechanism (examples include Ikeda and Apel 1981; Flierl et al. 1987; Spall and Robinson 1990; Spall 1995, hereafter S95; Samelson and Chapman 1995; Onken 1992; and Wood 1988; among others). The early growth periods in these models tend to agree well with linear theory. While the large amplitude behavior has some characteristics that agree well with observations, such as the ability to form separated vortices and the strength of the ageostrophic circulations, after several instability cycles these unforced fronts tend to evolve toward a baroclinic zone that is dominated by large amplitude eddies rather than a strong coherent jet, as was assumed for the initial state. This is often in contrast to the observed lifetimes of open ocean fronts that can greatly exceed the linear growth timescale. It will be shown here that the presence of a large-scale deformation field can maintain a strong baroclinic jet for long times, even in the presence of unstable waves and large amplitude meanders.

Linear stability theory often treats the development of time-dependent instabilities by assuming that the mean front is steady and two-dimensional, while allowing for small perturbations that have a wavelike structure in the horizontal (Pedlosky 1964). This results in an eigenvalue problem for the wave frequency, allowing for the possibility of a positive imaginary component and exponential growth of the small perturbations. Although the theory is only formally valid in the small amplitude limit, it is expected that these small amplitude perturbations will eventually grow to dominate the variability. However, the structure of fronts (and perturbations) associated with deformation fields are often not steady in time, particularly during the frontogenesis phase, and do not lend themselves to the separation of space and time inherent in the modal decomposition.

Recent theories have begun to address the stability of fronts in horizonal deformation. Dritschel et al. (1991) demonstrated that the presence of even weak horizontal deformation strongly influences the shear instability of a two-dimensional strip of constant vorticity. Sufficiently strong deformation fields ($f/4$) can effectively suppress the shear instability. Bishop and Thorpe (1994) find structures for optimal wave growth on a barotropic strip of vorticity whose amplitude increases with time under horizontal deformation. They find that, while perturbations generally experience a period of growth, the increasing aspect ratio of the perturbations that results from the deformation ultimately suppresses the intense growth that would be supported by normal mode instabilities in the absence of deformation. These studies conclude that deformation tends to strongly supress nonlinear wave growth for the problem of two-dimensional shear instabilities, suggesting that barotropic instability may not be an effective means to limit frontogenesis.

Bishop (1993, hereafter B93) applies a similar analysis to optimal wave growth in a uniform baroclinic shear under horizontal deformation. He finds once again that deformation generally tends to limit the maximum wave amplification, although it may enhance wave amplification for short periods of time relative to the unstrained case. He also provides an estimate for the time at which nonlinear terms, formally neglected in the theory, will become important, and notes that the leading order influence of nonlinear terms is to weaken the horizontal density gradient in the front. Joly and Thorpe (1991) consider the stability of time-dependent flows in dry and moist atmospheres, although they neglect the

alongfront stretching of the perturbation wavelength by the deformation field, a process shown by B93 to be important for quantifying the maximum wave amplification. Because these previous theoretical studies have been limited to the linear regime, there is no feedback mechanism between the growing waves and the time-dependent frontal structure and, hence, they can not provide a mechanism to counteract the frontal collapse.

The present study extends these previous essentially two-dimensional linear results into the three-dimensional large amplitude regime by allowing time-dependent instabilities to develop in the alongfront direction. The primary objective of this paper is to understand the fundamental consequences of a large-scale deformation on the stability, mean structure, and ageostrophic circulations of baroclinic fronts. The model configuration and forcing are presented in section 2. The steady two-dimensional frontal structure and resulting ageostrophic circulations are summarized in section 3. Aspects of the nonlinear three-dimensional regime are discussed in section 4, including the stabilizing influence of the deformation field and the emergence of time-dependent equilibrated states. These model results are compared with various oceanic observations in section 5, and final conclusions are given in section 6.

2. Model configuration

The model used for the present study is based on the semispectral primitive equation model described by Haidvogel et al. (1991). The primitive equations are appropriate for frontal studies such as the present one where the vertical component of relative vorticity $\zeta = v_x - u_y$ can be of the same order of magnitude as the planetary vorticity, the isopycnals may undergo large excursions in the vertical (often outcropping at the surface), and the vertical velocity may be greater than formally allowed in quasigeostrophic theory. A level, rather than an isopycnal layer, representation in the vertical has been chosen so that the vertical resolution in the model will be uniform across the front even in the presence of a cross-front gradient in stratification. While this may not be a concern for representing the large-scale geostrophic flow (whose structure is closely coupled to the density field), it does become important if one wants to accurately resolve the vertical structure of the ageostrophic velocity field in regions of weak stratification.

The model solves the primitive equations of motion, consisting of prognostic equations for the horizontal velocity field (u, v) and temperature (T), and diagnostic equations for the vertical velocity (w), the density (ρ), and the pressure (P). While the model formally uses terrain-following coordinates in the vertical and orthogonal curvalinear coordinates in the horizontal, the present application uses a standard, uniform Cartesian coordinate system with a flat bottom. The model equations and boundary conditions are given in the appendix, while further details can be found in Haidvogel et al. (1991) and the User's Guide to SPEM 5.1 (K. Hedstrom 1995, personal communication).

The model is configured in a regional domain in order to study the influences of a large-scale (relative to the baroclinic deformation radius) deformation field on the formation and maintenance of baroclinic upper-ocean fronts. The regional approach reduces the grid size required to model the frontal region, thus reducing computational costs and allowing for longer integrations at higher resolution than would otherwise be possible. More importantly, the strength of the deformation field may be specified and held constant in time. This allows one to attribute any time-dependent behavior to the dynamics inherent in the steadily forced system without the complications of time-dependent deformation fields or changing properties of the large-scale flow. It also allows for a comprehensive exploration of the frontal circulation as a function of the strength of the deformation field.

Frontal formation by large-scale deformation fields is relevant to a broad range of geophysical regimes spanning the sub-mesoscale to the gyre scale in both the atmosphere and the ocean. Motivated, in part, by this general applicability of the internally forced problem, external forcing (surface wind stress and buoyancy flux) and turbulent mixed layer physics have been neglected. For the specific case of the STCZ, the data analysis of H91 demonstrated that the wind-driven Ekman convergence was too small in magnitude to maintain the FASINEX fronts. It is noted that these neglected processes will, in general, be important for setting up the large-scale meridional density gradient and deformation field that define the initial and boundary conditions used here. Thus, the neglected processes are parameterized through the choice of boundary conditions. The present focus is on understanding the basic dynamics of the steadily, internally forced system.

The deformation field is purely barotropic; it is specified in the initial and boundary conditions through the barotropic streamfunction as

$$\psi = -\alpha xy. \tag{1}$$

This deformation field is an idealization of a confluent region as forced, for example, by gyre-scale recirculations or by the geostrophic flow between adjacent mesoscale eddies. Similar idealizations have often been used for two-dimensional frontogenesis studies (HB72; BOW88; MacVean and Woods 1980; and others). The boundary conditions are held fixed in time here largely as a simplification, although the large-scale deformation fields typically vary on a timescale much longer than either the frontogenetic timescale or the linear growth timescale.

The mean density field has an exponential decay with a vertical scale of 600 m. In the horizontal, the density is initialized with a weak meridional gradient at the surface, which decays linearly with depth to zero gra-

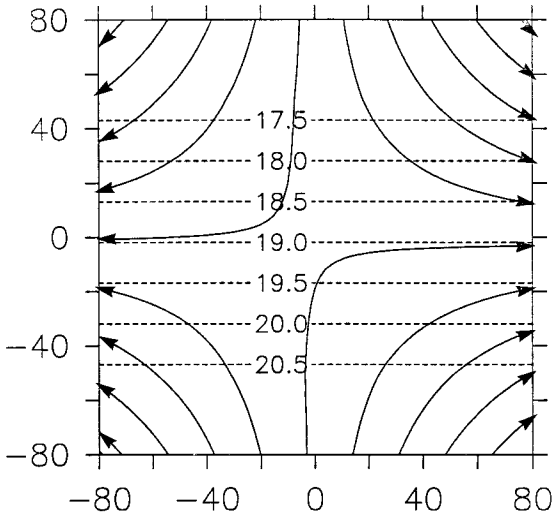

FIG. 1. Initial temperature field at 6-m depth (dashed lines) and barotropic transport streamfunction (solid lines, contour interval = 10^6 m^3 s^{-1}, arrows indicate flow direction) for $\Delta\rho = 0.47$ kg m^{-3} and $\alpha = -1 \times 10^{-6}$ s^{-1}.

dient at 200 m. (Although there is no distinction between east and north in the present *f*-plane model, meridional will be used to describe the across-front direction and zonal will be used to describe the alongfront direction.) The initial velocity field is specified to be in geostrophic balance with the initial density field. The reference velocity for the geostrophic calculation is chosen such that there is no barotropic transport induced by the density gradient. An example of the initial meridional temperature gradient at 6-m depth, together with the transport streamfunction, is shown in Fig. 1.

The horizontal grid spacing is 2 km for all calculations. The model domain in section 3 extends 160 km in the meridional direction and 20 km in the zonal direction. The horizontal extent of the model domain used in section 4 to study variation in the alongfront direction is 160 km in both the zonal and meridional directions. There are 12 grid points in the vertical located at depths 6, 18, 32, 47, 66, 90, 121, 164, 225, 313, 443, 635 m. The total depth of the model domain is 750 m with a flat bottom. (The central three-dimensional case has been repeated with 18 levels and produces essentially the same results.) The horizontal coefficients of diffusion and viscosity are 10 m^2 s^{-1} (unless otherwise noted), and the vertical coefficients of diffusion and viscosity are 1×10^{-5} m^2 s^{-1} for all calculations.

3. Two-dimensional steady solutions

The initial density distribution is a function only of depth and latitude. As such, unless some small perturbation is introduced in the zonal direction, the baroclinic structure will remain two-dimensional. This class of problems is similar to many previous calculations carried out formally in two dimensions (BOW88; Williams 1974; MacVean and Woods 1980) and studied analytically by HB72. This set of calculations is carried out here in order to form a basis for comparison with the three-dimensional results.

The model is integrated in time until a steady state is achieved. This steady solution is not possible in the inviscid analytic models, although steady balances were achieved in the atmospheric numerical studies of Williams (1974) and Gall et al. (1987). The analytic solution indicates that a discontinuity must form on the boundary because there is no mechanism to take heat vertically away from the boundary (zero vertical velocity and vertical diffusion) while the horizontal velocity field continually increases the cross-frontal density gradient there (HB72). The primary balance in the temperature equation for the present model is between the horizontal and vertical advection terms. The explicit horizontal diffusion is a maximum of a few percent, and the vertical diffusion is less than 1%, of the advective terms. Although nearly inviscid, this weak diffusion is still sufficient to halt the frontogenesis. However, the maximum alongfront velocity is not a strong function of the explicit horizontal diffusion in the model. It increases (decreases) by only 10% for a factor of 2 decrease (increase) in the horizontal viscosity and diffusion coefficients.

Meridional sections of the alongfront velocity (u), the temperature (T), the baroclinic cross-front velocity ($v' = v - V$, where v is the total meridional velocity and V is the depth averaged meridional velocity), and the vertical velocity (w) are shown in Fig. 2 for a case with $\alpha = -1 \times 10^{-6}$ s^{-1} and the surface density change across the front $\Delta\rho = 0.47$ kg m^{-3}. During the spinup from the initial conditions, the deformation field compresses the initially weak density gradient in the meridional direction and the zonal velocity accelerates due to the thermal wind relation. This acceleration continues until the meridional density gradient ceases to increase, resulting here in a maximum alongfront velocity of approximately 25 cm s^{-1} (Fig. 2a). A strong front in temperature is produced, with a maximum change in temperature at the surface of 3.35°C over a horizontal scale of less than 10 km (Fig. 2b).

The ageostrophic velocity field is large in the frontal region. Even though there is no zonal density gradient to support a geostrophic flow in the cross-frontal direction, the meridional velocity is not simply given by the barotropic deformation field. There is an ageostrophic response to the acceleration of the flow in the zonal direction (Fig. 2c), as previously discussed by HB72, MacVean and Woods (1980), BOW88, S95, and others. This flow is from the warm side of the front toward the cold side of the front in the upper ocean, with a compensating flow toward the warm side of the front in the deep ocean. There is also a development of ageostrophic vertical velocities in response to the change in relative vorticity as parcels are carried into and out of the frontal region (Fig. 2d). The conservation of potential vorticity

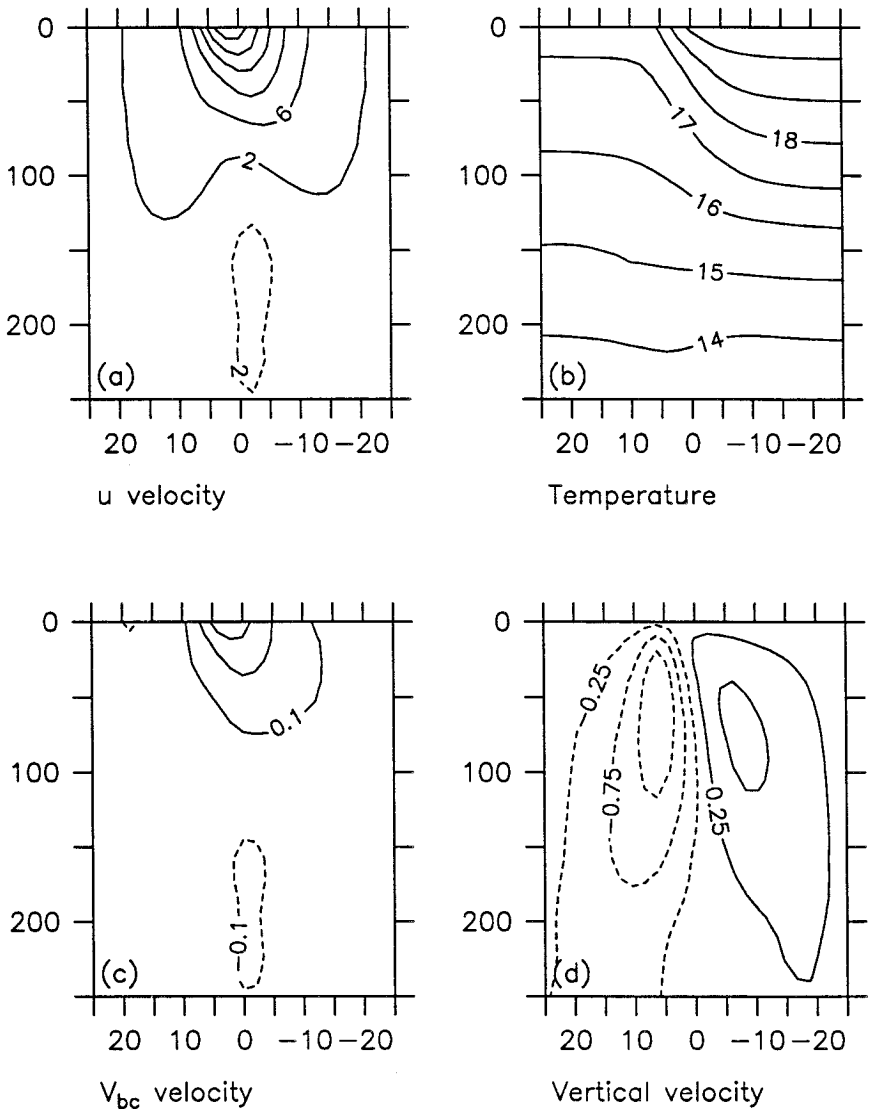

FIG. 2. Meridional sections of (a) alongfront velocity (cm s^{-1}), (b) temperature (°C), (c) baroclinic cross-front velocity (cm s^{-1}, see text for definition), and (d) vertical velocity (m day^{-1}) for the two-dimensional solution with $\Delta\rho = 0.47$ kg m^{-3} and $\alpha = -1 \times 10^{-6}$ s^{-1}.

requires that water parcels undergo stretching on the cold side of the front (positive relative vorticity) and compression on the warm side of the front (negative relative vorticity). The zero vertical velocity boundary condition at the surface gives rise to downwelling on the cold side and upwelling on the warm side. These ageostrophic velocities were also discussed in the previous frontogenesis studies by HB72, Bleck et al. (1988), S95, and others. This result is also consistent with several observational studies. For example, Voorhis and Bruce (1982) and Pollard and Regier (1992) estimated similar circulations in the North Atlantic STCZ, while Rudnick (1996) finds a similar pattern near the Azores Current.

While there is no net vertical mass flux driven by the ageostrophic circulation cell averaged over the frontal area, there is a net vertical heat flux because the upwelling water is always warmer than the downwelling water. This positive vertical heat flux is required to convert potential energy to kinetic energy as the parcels are carried into the baroclinic jet. The magnitude of this vertical heat flux is estimated from the magnitude of the vertical velocity as $Q = \rho c_p \Delta T w$, where ΔT is the temperature change across the front and c_p is the specific heat of seawater. Typical values for fronts found in the FASINEX experiment are $\Delta T = 2$°C, $c_p = 4 \times 10^3$ J kg^{-1} K^{-1}, $\rho = 10^3$ kg m^{-3}, and $w = 1$ m day^{-1}. In order to compare this value with the climatological surface heat flux the frontal contribution must be averaged over the horizontal length scale of the mesoscale eddies that are supplying the deformation field. If one assumes that there exists one front in each confluent region between

eddies, then a factor of $L_f/L_e \approx 1/30$ is introduced, where L_f is the width of the mixed layer front and L_e is the diameter of the mesoscale eddies. This gives a net large-scale vertical heat flux of $O(3\ \mathrm{W\ m^{-2}})$. While crude, this estimate indicates that the vertical heat flux due to the frontal ageostropic circulation is of the same order of magnitude as the climatological net annual surface heat flux in the subtropical gyre interior (see also section 4d).

In principle, the inviscid ageostrophic vertical circulation cell is reversible. This means that the net upward vertical heat flux experienced in the confluent regions would be exactly balanced by a downward vertical heat flux in diffluent regions. However, the timescales associated with these two regimes are quite different. The frontal region is characterized by large relative vorticities and large upwelling and downwelling rates, giving short residence times for parcels in the upper ocean. The diffluent regions would instead be characterized by very small relative vorticities spread over large areas, giving rise to very small amplitude vertical velocities. Thus, while the parcels are upwelled or downwelled very quickly in the frontal region, it takes much longer for them to be returned to their original depth away from the fronts. This would give external forcing (neglected here) a chance to interact with the upper ocean and remove the net heat gain experienced in the frontal region. Although a detailed analysis is beyond the scope of this paper, the disparity in timescales between the frontal region and the diffluent regions suggests that there may be a net large-scale average vertical heat flux resulting from the frontal dynamics.

In a related manner, we would expect these frontal regions to be locations of subduction, where water parcels are removed from the surface boundary layer into the stratified interior. This mechanism for frontal subduction is fundamentally different from the subduction forced by baroclinic instability discussed by S95. An upper bound for the local subduction rate is given by the vertical velocity. To compare this with large-scale processes such as Ekman pumping or horizontal shoaling of the mixed layer, this needs to be averaged over large horizontal length scales, introducing a factor of L_f/L_e. This scale factor would then give averaged subduction rates for the FASINEX-like fronts of 10 m $\mathrm{yr^{-1}}$, similar to the net annual Ekman pumping rate and estimates for the lateral induction term (Marshall et al. 1993) and also similar to that resulting from baroclinic instability of an unforced FASINEX-like front (S95).

4. Three-dimensional solutions: Instabilities and nonlinear equilibration

a. Instabilities and self-sustaining oscillations

The possibility of variability in the alongfront direction is now considered by extending the model domain to 160 km in both the zonal and meridional directions. The model has been initialized with a broad baroclinic zone, as in the previous section, but now small amplitude perturbations at zonal wavelengths between 30 km and 160 km have been added to the initial meridional density gradient. The model was then integrated in time until a steady state, or statistically steady state in the case of time dependence, was achieved. The solutions are classified here as steady if the zonally averaged root-mean-square perturbation amplitude remains less than 10% of the baroclinic deformation radius, although all time-dependent solutions here had perturbation amplitudes on the order of the deformation radius or greater. The solutions are never completely steady, however, as the imperfect boundary conditions act as a continual source of small-scale noise to the system. The Froude number is generally less than 1 so that this information is able to propagate from the boundaries into the interior.

For sufficiently strong deformation fields the steady, two-dimensional solutions found in the previous section are recovered. However, for weaker deformation fields the frontal region developes large amplitude, time-dependent meanders. This transition from the steady two-dimensional regime to the time-dependent three-dimensional regime is indicated in Fig. 3 by the width and Richardson number of the averaged front as a function of the deformation strength α for a fixed value of $\Delta\rho = 0.47\ \mathrm{kg\ m^{-3}}$. All alongfront averages are taken in frontal coordinates, defined as the position of the 18°C isotherm at 32-m depth. The width of the front is defined as the distance between the 17.5°C and 20.25°C isotherms at 6-m depth. For $|\alpha| \geq 1.25 \times 10^{-6}\ \mathrm{s^{-1}}$ (Fig. 3a) the width of the three-dimensional front is the same as that for the two-dimensional case. However, as the deformation strength is further reduced, the width of the three-dimensional front becomes greater than for the two-dimensional solutions. These are also those cases that develop time-dependent meanders.

Similarily, the mean Richardson number of the front in these time-dependent cases is greater (reflecting weaker vertical shear in the alongfront velocity) than that found in the absence of instabilities (Fig. 3b). The local Richardson number of the mean front can be much less than this large-scale mean and is generally a minimum of ~ 5 near the upper ocean on the cyclonic side of the front. The minimum Richardson number of the synoptic flow fields is generally less than 1, suggesting that enhanced turbulent mixing, neglected here, may become important in these regions.

These results suggest that the resolved eddy fluxes due to baroclinic instability are at least partially limiting the intensity of the mean front. The subgrid-scale mixing parameterization is also active in limiting further jet intensification, particularly in regions of locally enhanced horizontal shear. The calculation that first shows strong time dependence will now be considered in more detail ($\alpha = -1 \times 10^{-6}\ \mathrm{s^{-1}}$, referred to as the central case). This value of the deformation field is close to

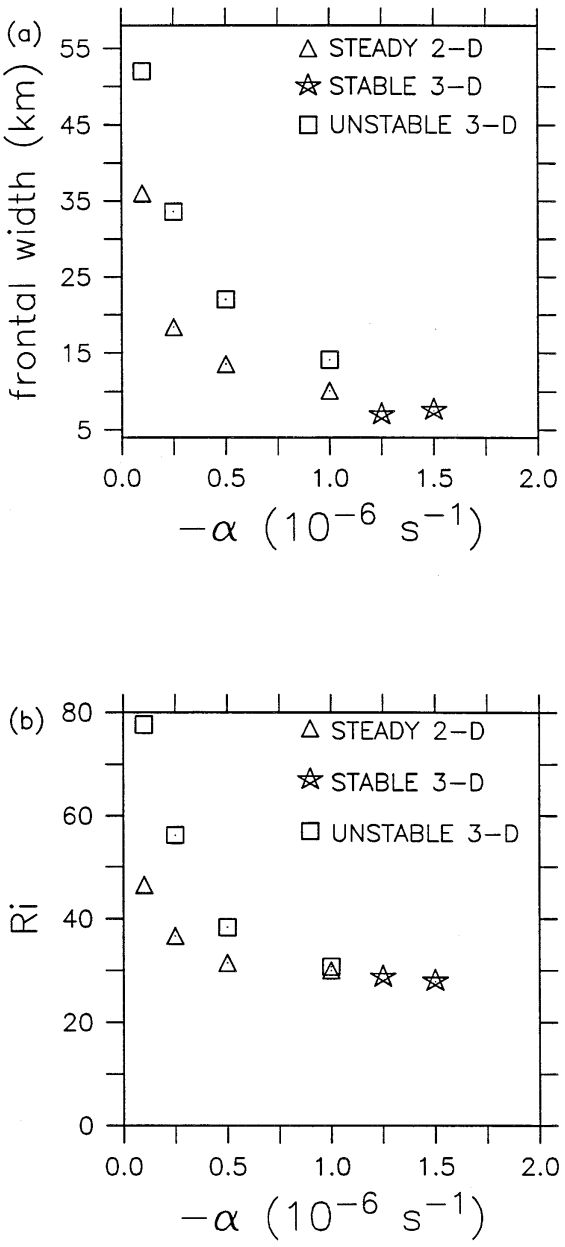

FIG. 3. (a) Frontal width and (b) Richardson number (Ri) as a function of the deformation strength α for $\Delta\rho = 0.47$ kg m^{-3}. Ri = $(N/U_z)^2$, calculated over a vertical scale of 150 m and averaged over the deformation radius in the horizontal. Symbols indicate stable three-dimensional (stars), steady two-dimensional (triangles), and unsteady three-dimensional (squares) results.

estimates of the strength of the deformation field provided by thermocline mesoscale eddies in the North Atlantic STCZ (Bisagni 1991; MacVean and Woods 1980; H91; H97).

A synoptic view of the upper-level velocity, temperature, and transport streamfunction is shown in Fig. 4. While the frontal region varies considerably over the duration of the calculation, this example demonstrates typical meander scales, frontal features, and behavior near the open boundaries. The frontal region is characterized by a strong baroclinic jet with meanders of approximately 20-km amplitude and 70-km wavelength. There is considerable alongfront variation in the baroclinic structure, with jet intensification along the upstream side of the troughs and a weakening of the jet near the meander crests (see the next section for more discussion on the structure of the baroclinic waves). The large-scale deformation field is clearly visible away from the frontal region. The transport streamfunction shows only a small perturbation from its original uniform deformation (recall that the jet was initialized such that there was no barotropic component). The model is generally well behaved near the boundaries, although the small-scale noise along the jet near the right-hand boundary shows evidence of errors propagating into the interior.

The time series of the meander amplitude and the maximum jet velocity (averaged in frontal coordinates in the alongfront direction) for the central case indicates that the frontal region reaches a statistical equilibrium with oscillations about the mean state (Fig. 5a). The meander amplitude (nondimensionalized by the deformation radius $L_d \sim 6.5$ km) is defined by the root-mean-square deviation of the jet axis from a purely zonal flow. The small perturbations grow to approximately the deformation radius in amplitude over the first few nondimensional time units. The rms meander amplitude then oscillates between approximately $0.5L_d$ and $1.5L_d$ with a period of approximately 3α, or near 30 days for this case. The maximum velocity at the core of the jet averaged in frontal coordinates (normalized by $L\alpha$) shows a similar oscillation. The maximum jet velocity increases from about 0.5 (8 cm s^{-1}) in the initial conditions to oscillate between 1.2 and 1.5 (20–25 cm s^{-1}). The period of the oscillation is very close to that for the meanders with a tendency (although not always true) for the velocity to be nearly out of phase with the meander amplitude. The baroclinic zone may be characterized as oscillating between a relatively straight jet with large vertical shear (maximum velocity) and a relatively meandering jet with smaller vertical shear.

Similar low-frequency oscillations are found for all integrations for which large amplitude instabilities develop (see section 4c for unstable regime). For calculations near the critical deformation sufficient to suppress large amplitude meander growth, the oscillations are characterized by single wave events that grow to large amplitude and propagate out of the domain. As the strength of the deformation is reduced, the amplitude of the meanders increases and the period of the oscillations broadens to include both higher and lower frequency components, as indicated in Fig. 5b for $\alpha = -0.5 \times 10^{-6}$ s^{-1}. (Note that the dimensional duration of the model integration is now 800 days, twice as long as in the previous calculation.) The periods of large amplitude meandering are no longer simply described

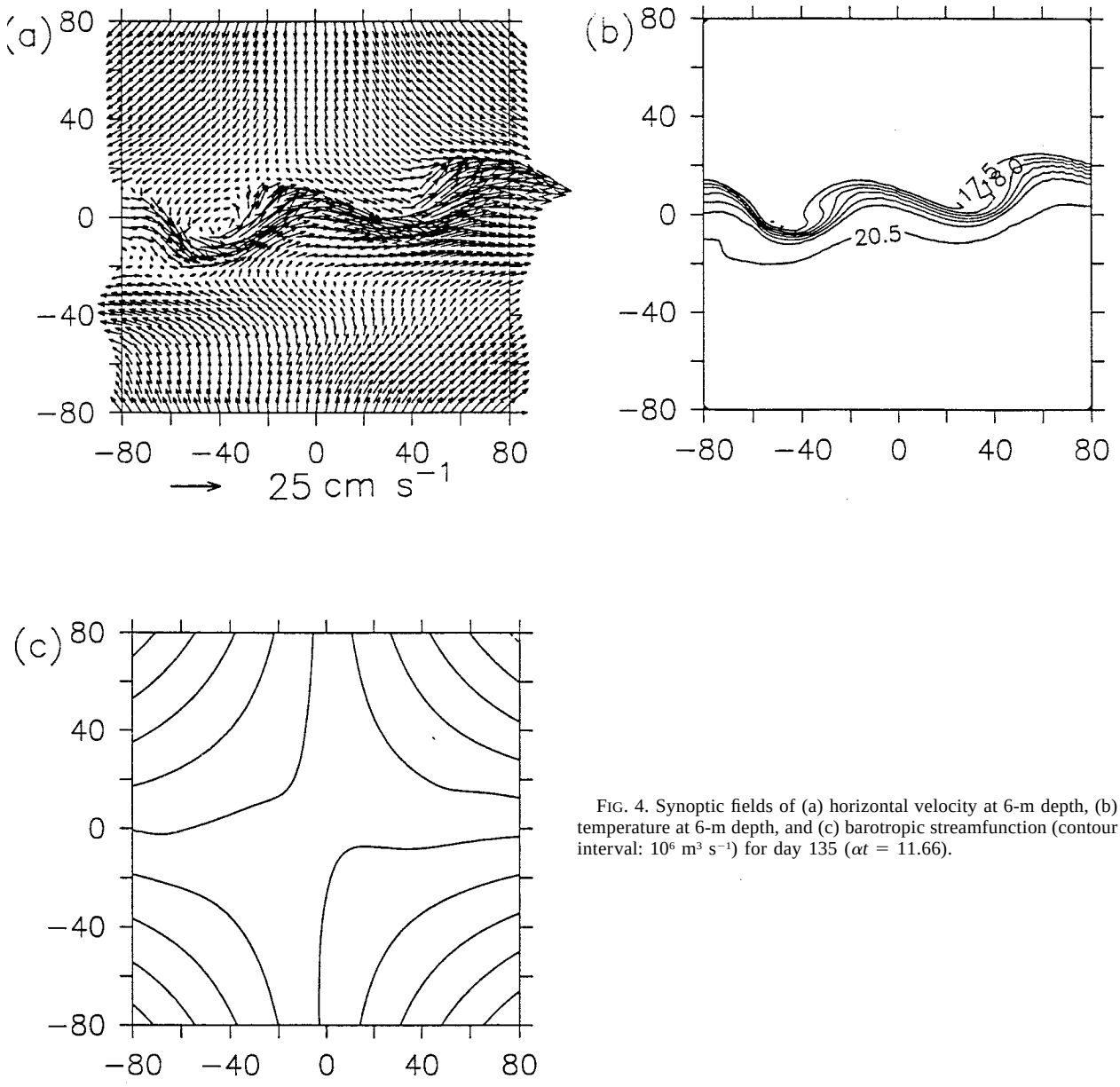

FIG. 4. Synoptic fields of (a) horizontal velocity at 6-m depth, (b) temperature at 6-m depth, and (c) barotropic streamfunction (contour interval: 10^6 m^3 s^{-1}) for day 135 (αt = 11.66).

as single wave growth–propagation events but now contain several baroclinic wave cycles of different wavelengths and amplitudes. Although it is unlikely that the external deformation field provided by mesoscale eddies would remain steady for such long time periods (as is assumed here), individual mesoscale eddies can be identified under surface fronts for periods of 200 days (Bisagni 1991) and gyre-scale recirculations probably persist for even longer periods. In addition, the identification of such low-frequency behavior of the baroclinic jet reveals aspects of the nonlinear equilibration dynamics that are relevant to the process of frontolysis, as discussed further in the following sections.

This oscillating behavior is fundamentally different from the behavior one finds for frontal calculations in a periodic channel in the absence of a deformation field. This is demonstrated in Fig. 5a by a calculation that was restarted from the density field of the central calculation on day 30 (αt = 2.6) with α = 0.0. The unforced case begins to diverge from the forced case immediately, bringing into question the relevance of even short time periodic channel calculations for fronts that exist in the presence of deformation fields. In this unforced case, the frontal instabilities continue to grow on the Eady timescale $\tau_e \propto \mathrm{Ri}^{1/2}/f$, where $\mathrm{Ri} = (N/U_z)^2$ is the Richardson number, typically $O(10–100)$ for oceanic frontal regions. The meanders grow to very large amplitude and form pinched off vortices (indicated by dis-

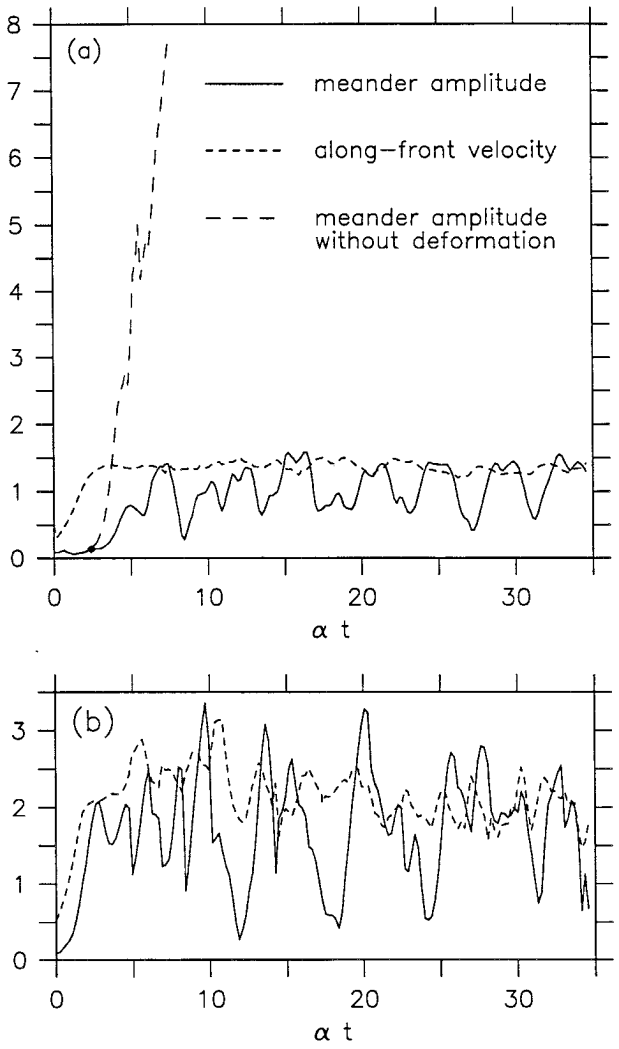

FIG. 5. Time series of root-mean-square meander amplitude (solid line, nondimensionalized by the deformation radius) and maximum alongfront velocity averaged in frontal coordinates (short dashed line, nondimensionalized by $-L\alpha$) for $\Delta\rho = 0.47$ kg m^{-3} and (a) $\alpha = -1 \times 10^{-6}$ s^{-1}, (b) $\alpha = -0.5 \times 10^{-6}$ s^{-1}. The long dashed line in (a) is the meander amplitude for a periodic channel calculation restarted with $\alpha = 0$ at $\alpha t = 2.6$

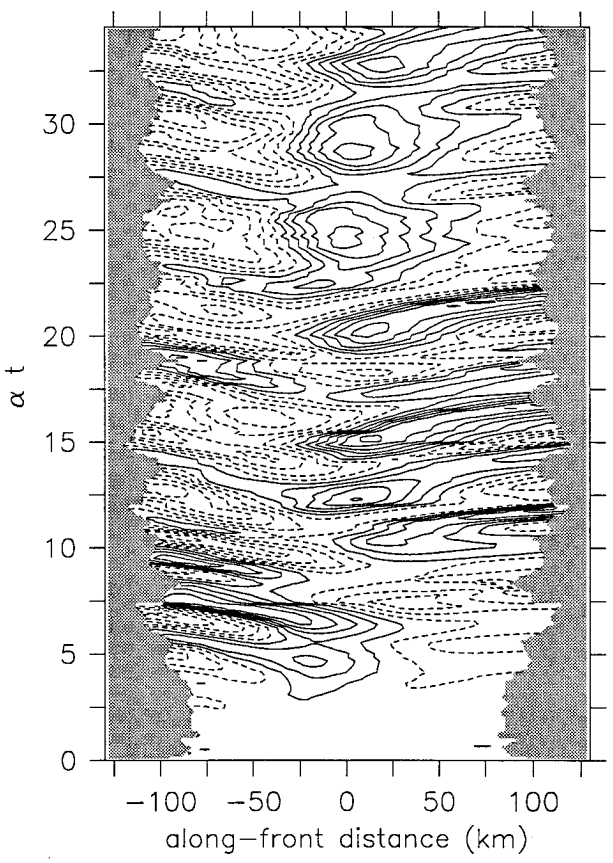

FIG. 6. Meander amplitude as a function of alongfront distance and nondimensional time for the central case, contour interval: 0.5.

ruptions to meander growth at $\alpha t = 4.8, 5.7$). After 60 days of integration ($\Delta\alpha t = 5.18$), the frontal region consists of a collection of eddies rather than a coherent frontal jet. This is in contrast to many observations, which indicate that open ocean and atmospheric frontal regions can persist for many eddy instability cycles, sometimes exhibiting very little meandering for extended periods (e.g., H91 and Bisagni 1991). The fronts under deformation studied here persist as strong coherent features for the duration of the experiments (up to 1400 days), well beyond the Eady timescale that characterizes the breakdown of similar fronts in either a periodic channel or a domain with a specified frontal structure at the inflow to the region (S95). For fronts relevant to the oceanic parameter range, the large amplitude frontal behavior is fundamentally altered for deformation fields as small as 10^{-7} s^{-1} (see the next section). The unforced spindown problem is still appropriate, however, for situations in which the deformation field disappears after some period of frontogenesis.

b. Baroclinic wave cycle

The nature of the meander growth and decay during these oscillations is indicated by the meander amplitude as a function of time and the alongfront distance (Fig. 6). This presentation provides an efficient means to view the time-dependent behavior of the front. A plot of the temperature at a given latitude versus time would show a similar behavior because the meander amplitude is closely coupled to the horizontal displacements of the isotherms. The meander amplitude is preferred because it may be nondimensionalized by a relevent length scale and it allows one to track meander propagation events even in the presence of large-scale shifts in the frontal position.

Aside from the very early period, the frontal region is characterized by a series of developing and propagating waves. They generally begin to develop in the model interior and increase in amplitude as they prop-

agate toward the model boundaries. The peak amplitude is often reached within the model interior with subsequent decay as the waves leave the domain. The rate at which the meanders propagate toward the boundaries increases as the boundary is approached in both the positive and negative zonal directions. Near the center of the domain there is very little zonal propagation. This is what would be expected for propagation that is controlled by the large-scale deformation field, $U = -\alpha x$. A consequence of this is that the zonal wavelength of the perturbations increases in time as the waves are stretched by the deformation field (see also B93 and the following section). This time-dependent behavior of the perturbation wavelength indicates that a space–time decomposition of the perturbation structure is not appropriate. When the meanders are at large amplitude, the alongfront length integrated over the zonal extent of the basin is large (corresponding to the large meander amplitude events in Fig. 5). After the meanders propagate out of the domain, the next cycle of wave growth is started with a series of small amplitude, short wavelength perturbations. For this model calculation, the low-frequency oscillation in the state of the frontal region corresponds to one cycle of wave growth and decay, however, as discussed in the previous section, for other values of α and $\Delta\rho$ there can be more than one cycle of meander growth between small amplitude meander states.

The structure of the geostrophic and ageostrophic velocity field in the meanders is typical of that found for large amplitude baroclinic waves in the atmosphere (see, e.g., Hoskins and Pedder 1980) and ocean (Voorhis and Bruce 1982). The geostrophic velocity field at 6-m depth is shown in Fig. 7a for a portion of the model domain on model day 74 ($\alpha t = 6.4$). The maximum velocity in the jet is approximately 30 cm s^{-1}. The presence of the deformation field is clear away from the front. The meander has grown to approximately 20 km in amplitude and is beginning to break backward around the strong cyclonic circulation in the trough. The cyclonic circulation provides a region of convergent horizontal deformation along the upstream side of the trough that dominates over the larger-scale imposed deformation of strength α. This convergence enhances the horizontal density gradient upstream of the troughs (see also Fig. 4). The geostrophic flow is advecting the cold water to the south in the trough and the warm water to the north in the crest, intensifying the meander amplitudes. This is typical of the frontal meandering that has motivated many of the previous studies of frontogenesis (HB72; S95).

The horizontal ageostrophic velocity field is shown in Fig. 7b superimposed on the temperature field at 6-m depth. The ageostrophic circulation is advecting warm water to the north in the meander crest and along the upstream side of the deepening trough, and cold water toward the south between the crest and trough. The ageostrophic flow opposes the geostrophic flow in regions of cyclonic vorticity, and is in the same direction as the geostrophic flow in regions of anticyclonic vorticity, consistent with gradient wind balance. The vertical velocity at 66-m depth (Fig. 7c) is consistent with this ageostrophic near-surface flow. This pattern of upwelling just downstream of the developing low (the cylonic circulation in the trough) and downwelling just upstream of the trough is very similar to that discussed by Hoskins and Pedder (1980) and is as expected from basic baroclinic instability theory (Holton 1979, pp 140–143). This ageostrophic horizonal and vertical velocity pattern and amplitude are also consistent with what one would expect based on the local acceleration and deceleration of parcels in the upper ocean as they flow along the frontal path (Hoskins and Pedder 1980; Onken 1992; S95). The region upstream of the trough has an enhanced cross-frontal density gradient resulting from the local deformation field provided by the cyclonic circulation, giving rise to an acceleration in the alongfront velocity and downwelling along the cold side of the front. Subgrid-scale mixing is enhanced in these strong gradient regions. A similar situation arises just downstream of the crest, while upwelling is found in the region of deceleration at the crest.

This northward heat flux is as expected for a baroclinically unstable wave and plays an important role in balancing the steepening of the front provided by the deformation field. The large-scale deformation increases the potential energy of the frontal region by steepening the isopycnal slopes, while the release of potential energy from the front through large amplitude baroclinic wave events converts this mean frontal potential energy into wave potential and kinetic energy. The wave energy then propagates out of the confluent region through the ends of the model domain.

The ability of the front to form pinched off vortices is greatly reduced by the presence of the large-scale deformation field. S95 found that, in the absence of a deformation field, baroclinic dipole pairs were formed during the breakdown of a similar baroclinic frontal zone and that they were able to carry heat (and other properties) far from the frontal region. The deformation field both limits the maximum meander amplitude (Fig. 5) and advects density anomalies back into the frontal region so that, for all but very small values of α, most of the heat flux is carried in patches of ageostrophic cross-frontal velocities, not isolated coherent vortices, and is limited to the near frontal region.

c. Nonlinear equilibration

The theory of the instability of time-dependent flows is helpful for understanding the nature of the equilibrated state and to predict what flows will ultimately be rendered steady or unsteady in equilibration. B93 developed a linear model for maximum wave amplification

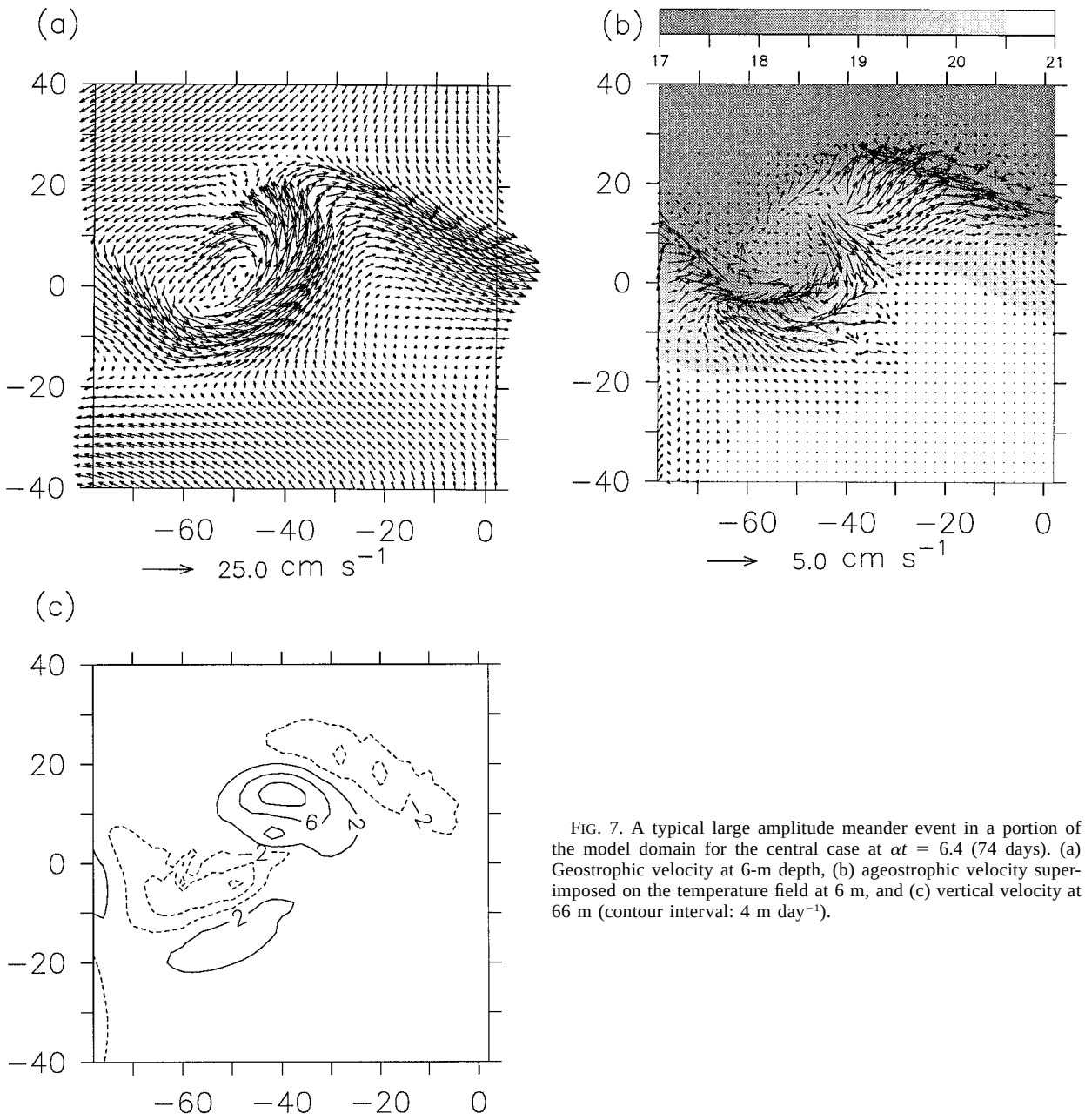

FIG. 7. A typical large amplitude meander event in a portion of the model domain for the central case at $\alpha t = 6.4$ (74 days). (a) Geostrophic velocity at 6-m depth, (b) ageostrophic velocity superimposed on the temperature field at 6 m, and (c) vertical velocity at 66 m (contour interval: 4 m day^{-1}).

for baroclinic flows in a horizontal deformation field. The approach makes use of the conceptual model of Hoskins et al. (1985) that interprets baroclinic instability in terms of counterpropagating Rossby waves. Bishop found that perturbations could undergo periods of growth while the baroclinic zone intensifies under deformation, and that the deformation ultimately limits growth by increasing the aspect ratio of the zonal and meridional wavelengths of the growing waves. Optimal wave amplification is found for perturbations that remain nearly 90° out of phase in the vertical and that have a large vertical length scale. While the maximum amplification can, at times, exceed the growth rate predicted by normal mode stability analysis (which is applicable only in the absense of a time-dependent mean state), the ultimate fate of all waves in this linear theory is that they must stop intensifying and propagate out of the region. Because there is no feedback between the waves and the intensifying baroclinic zone, there is no mechanism to stop the eventual collapse of the frontal region.

In the wave growth model of B93, the wave amplitude A is proportional to $e^{\gamma(t)}$, where the time evolution of γ is governed by the following equations:

$$\frac{\partial \gamma}{\partial t} = S \sin(\Theta) \tag{2}$$

$$S(k, l) = \left(\frac{f\Delta b}{\pi}\right)\left(\frac{lk}{\mu \sinh(\mu)}\right) \tag{3}$$

$$\frac{\partial \Theta}{\partial t} = S[2 \cosh(\mu) - \mu \sinh(\mu) + 2 \cos(\Theta)]. \tag{4}$$

The phase difference between the upper and lower boundary given by Θ, k, and l are the alongfront and across-front wavenumbers (nondimensionalized by the deformation radius), and $\mu^2 = k^2 + l^2$. Here S is a measure of the vertical scale height of the perturbations. The nondimensional density change across the baroclinic zone Δb is defined by

$$\Delta b = \frac{\pi U_0}{f L_d l_0}, \tag{5}$$

where U_0 is the initial maximum zonal velocity in the baroclinic zone, $L_d = NH/f$ is the internal deformation radius, and l_0 is the initial nondimensional meridional wavenumber (taken here to be $l_0 = 2\pi NH/fL_i = 0.628$ for all calculations, where L_i is the initial width of the baroclinic zone).

It is important to note that, in the linear theory, the dynamic constraints placed on the perturbation wave numbers require that they evolve with the deformation field as

$$k = k_0 e^{\alpha t}, \; l = l_0 e^{-\alpha t}. \tag{6}$$

This is qualitatively consistent with the zonal wavelengths of the growing meanders apparent in Fig. 6. As noted by B93, the decreasing horizontal scale of the front and increasing zonal length scale of the waves tends to stabilize perturbations by decreasing the meridional wavelength; while through thermal wind the decreasing meridional scale of the front results in an increasing vertical shear, tending to destabilize the front. As time becomes large, $l \to \infty$ and $k \to 0$ so that $S \to 0$ and $\partial\gamma/\partial t \to 0$ and all perturbations must stop intensifying.

Equations (2)–(6) quantify the physical interpretation of interacting Rossby waves proposed by Bretherton (1966) and Hoskins et al. (1985). This general system takes advantage of the fact that any linear wave solution may be represented as the sum of two linearly independent solutions. The two independent solutions chosen here are upper and lower boundary Rossby waves, each of which satisfies the upper and lower boundary conditions. These boundary waves do not propagate in isolation, but rather they each influence both the phase speed and amplification of the other wave. This can be simply understood if one considers two waves 90° out of phase in the vertical with the lower wave leading the upper wave. The maximum northward (southward) meridional velocity of the lower wave will occur at the downstream position of the meander crest (trough) of the upper wave. In this configuration, the lower wave will advect the meander crest (trough) to the north (south), thus resulting in an increase in the amplitude of the upper wave. The upper wave will have a similar impact on the lower wave. This interaction depends on two aspects of the flow; the vertical scale height of the waves (S, maximum growth is achieved when the scale height is the same for both waves) and the phase relationship between the two waves (Θ). It is easy to see that this interaction will be maximized when $\Theta = 90°$ and when the penetration scale of the boundary waves is large compared to the depth of the fluid ($S \to 1$). The stratification, wavenumbers, and Coriolis parameter all combine to determine the decay scale of the waves, those that decay rapidly away from the boundary will have little interaction with the other boundary and, hence, little capacity for growth. The above equations simply follow this mutual wave interaction in time, recognizing that the phase relationship between the two waves Θ and the vertical scale height (or wavenumbers k and l) may change in time. The traditional normal mode solution is obtained if one requires that the phase relationship and wavenumbers are fixed in time.

For baroclinically unstable flows, the kinetic and potential energy for the growing waves is derived from the potential energy of the mean flow. In the linear theory the wave amplitude is assumed to be too small to extract enough energy to significantly alter the mean state. However, if the waves grow to a large enough amplitude during their growth phase so that the nonlinear terms become important, they may alter the potential energy and, hence, the stability characteristics of the basic flow. As the potential energy of the mean state is lost to the growing perturbations, the isopycnal slopes in the frontal region are decreased and, through thermal wind, the vertical shear is also decreased. This conversion from potential energy to kinetic energy also reverses the cascade of increasing meridional wavenumber because the width of the frontal region increases. This is important for allowing future wave growth because a limiting factor in the maximum wave amplification under the linear theory is the ever-increasing meridional wavenumber l. (In the nonlinear primitive equation model the subgrid-scale mixing parameterization also limits the maximum meridional wavenumber.)

The magnitude of the nonlinear terms depends on the amplitude, and rate of change of the amplitude, of the perturbations. B93 estimates that the nonlinear terms will become important when the maximum amplitude of the developing waves (A_m) exceeds a threshold value A_0, given by the following expression:

$$\frac{\pi^2}{4}\phi^2(A_0^2 - 1) > \epsilon. \tag{7}$$

The amplitude of the initial perturbation, relative to the cross-frontal density change, is ϕ, and ϵ is a nondimensional measure of the size of the nonlinear terms. For details the reader is referred to B93.

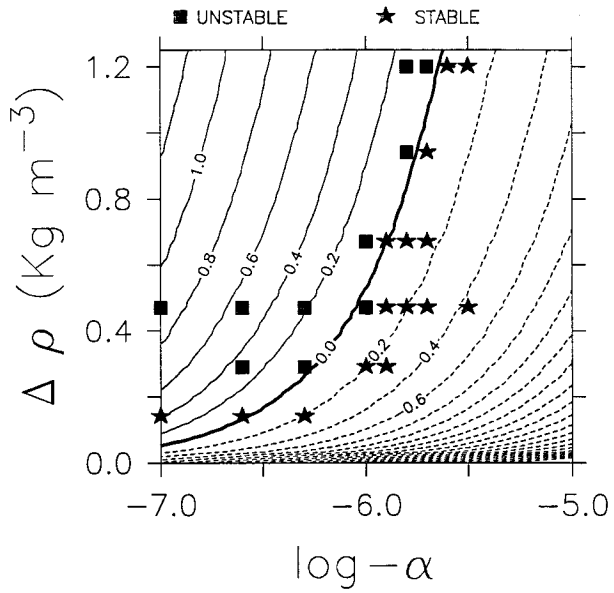

FIG. 8. Maximum wave amplification [$\log(\gamma/\gamma_0)$] as a function of the strength of the deformation field and the density change across the front, calculated from Eqs. (2), (3), and (4). The amplification has been normalized by $\gamma_0 = 2.66$, the value at which Eq. (7) predicts the nonlinear terms to exceed the threshold value of $\epsilon = 0.2$. It is expected that the nonlinear terms will become important in the region of solid lines, while the flow will remain linear in the region of dashed lines. The symbols indicate whether the final state of the nonlinear primitive equation model was found to be stable (stars) or unstable (squares).

The maximum wave amplification [$\log(\gamma_m/\gamma_0)$, where $A_m = e^{\gamma m}$ and $A_0 = e^{\gamma 0}$] is shown in Fig. 8 as a function of the density change across the front (related to U_0 through the thermal wind relation) and the strength of the deformation field. The initial zonal wavelength of the perturbation (k_0) was chosen to obtain maximum wave amplification, while the initial phase shift from the upper to the lower boundary $\Theta = 0$, consistent with how the primitive equation perturbations were initialized. (The results are not very sensitive to this choice, optimizing the initial value of Θ results in only a small increase in γ_m.) The maximum wave amplification γ_m was calculated from Eqs. (2), (3), and (4), where the period of integration was five nondimensional time units. This was found to be sufficient to reach the maximum wave amplitude in all cases. The amplification contoured in Fig. 8 has been normalized by $\gamma_0 = 2.66$ ($A_0 = 14.27$), the value at which the nonlinear terms become important. This threshold value was obtained from Eq. (7), assuming an initial perturbation amplitude $\phi = 1/50$ (as used for the primitive equation model initialization) and $\epsilon = 0.2$.

The results demonstrate that increasing the strength of the deformation field suppresses the maximum wave amplification, while decreasing the density change across the front also results in decreased wave amplification. Maximum wave amplification can be strongly suppressed for all values of $\Delta\rho$ if the deformation is strong enough. The physical interpretation of this result is that large α changes the wavenumber of the perturbations so rapidly [Eq. (6)] that no waves can spend enough time in a configuration that is conducive to growth such that large amplitude can be reached.

The values of α shown in Fig. 8 span several oceanic regimes. Gyre-scale deformation fields, such as the recirculation gyres north and south of the Gulf Stream, have deformation fields of $O(10^{-7}\ s^{-1})$. The transient deformation fields supplied by mesoscale eddies, such as observed in the FASINEX region of the STCZ, have deformation strengths of $O(10^{-6}\ s^{-1})$. Small, highly time-dependent, submesoscale eddies often found near the FASINEX mixed layer fronts have very strong deformation fields of $O(10^{-5}\ s^{-1})$. For these strongest deformation fields, all large amplitude meander growth is effectively suppressed. We can expect that the linear theory will hold well in the region of dashed lines, large α, and small $\Delta\rho$, while the nonlinear terms are likely to become important in the region of solid lines, smaller α, and larger $\Delta\rho$. The quantitative value of γ_m is influenced somewhat by the choices of ϵ, ϕ, L_d, and l_0 but, more importantly, the functional dependence of the wave growth and the transition to the nonlinear regime on α and $\Delta\rho$ are essentially the same for all reasonable parameter values.

A series of 25 nonlinear primitive equation model calculations have been carried out in which the density change across the baroclinic zone has been varied from 0.14 kg m^{-3} to 1.2 kg m^{-3} and deformation strength has been varied from $\alpha = -1 \times 10^{-7}\ s^{-1}$ to $-3 \times 10^{-6}\ s^{-1}$. (Note that, for numerical stability, the subgrid-scale mixing coefficient has been increased to 25 $m^2\ s^{-1}$ for all cases with $\Delta\rho \geq 0.67$ kg m^{-3}.) The nature of the equilibrated state for each of the calculations is indicated on Fig. 8, squares are for calculations that develop large amplitude waves and reach a time-dependent statistical steady state, while stars mark those calculations that are steady in their equilibrated state (reproducing the two-dimensional results from section 3). There is generally good agreement between those calculations for which the model exhibits time-dependent meandering and the parameters for which the nonlinear terms are predicted to be large.

This result, together with the increase in frontal width when instabilities are permitted, the time-dependent evolution of the meander wavelength being consistent with Eq. (6), the ageostrophic cross-frontal heat flux, and the oscillating nature of the equilibrated state, supports the interpretation that growing (nonmodal) waves and the resulting nonlinear feedbacks on the large-scale baroclinic flow help to limit the frontogenesis in the baroclinic zone.

It is noted here that the vertical shear is assumed to be uniform between upper and lower boundaries in the model of B93, while in the primitive equation integrations the vertical shear is surface intensified. The

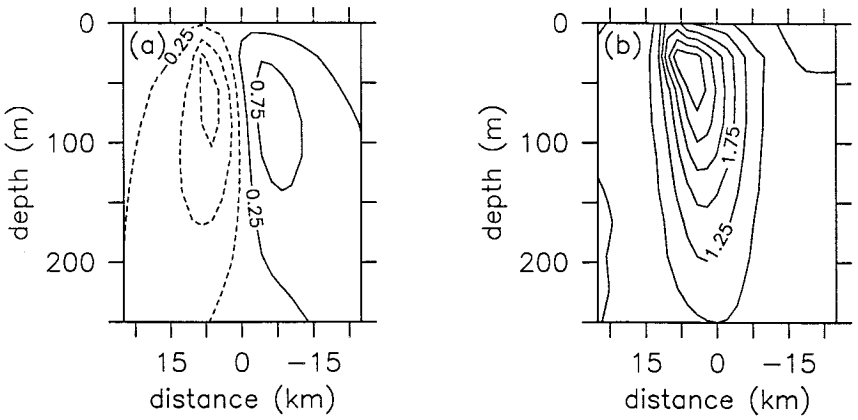

FIG. 9. (a) Vertical velocity averaged in frontal coordinates (m day^{-1}); (b) root-mean-square perturbation vertical velocity relative to (a) (m day^{-1}) for the central case.

decreased vertical scale in the surface-intensified model will tend to decrease the maximum wave amplification compared to the uniformly sheared case. Thus, while exact comparisons with Bishop's analytic model and the primitive equation model are probably not justified, the qualitative behavior of the shear instability is consistent with the instability mechanism in the nonlinear model.

The subgrid-scale mixing parameterization in the model impacts the wave development in two ways. By suppressing wave growth, it influences the quantitative value of the minimum deformation strength required for transition to three-dimensional solutions. For example, an increase in the diffusion coefficient from 10 to 20 m^2 s^{-1} shifts the transition to time-dependent equilibrated states for $\Delta\rho = 0.47$ kg m^{-3} from between 1×10^{-6} and 1.25×10^{-6} s^{-1} to between 0.5×10^{-6} and 1×10^{-6} s^{-1}. Decreases in the diffusion coefficient were not possible due to numerical stability constraints, but it is anticipated that a weaker subgrid-scale mixing would shift the transition point toward stronger deformation fields. The linear theory of Bishop, however, indicates that even in the inviscid limit the wave amplification will be limited by the deformation field in a manner qualitatively similar to that found here for weak diffusion. The subgrid-scale mixing also limits the frontal enhancement in regions of locally intense frontogenesis associated with large amplitude baroclinic waves. It is recognized that the quantitative behavior of the fronts studied here will be sensitive to the particular choice of subgrid-scale mixing; however, it is expected that the qualitative influence of the large-scale deformation fields on such baroclinic fronts will remain an important part of the frontal evolution for weakly diffusive systems.

d. Vertical velocity and vertical heat flux

The mean geostrophic and ageostrophic velocity structures in the three-dimensional solutions look very much like those in the two-dimensional solutions discussed in the previous section, as indicated by the mean vertical velocity for the central case in Fig. 9a. The mean vertical velocity calculated in spatially fixed Eulerian coordinates greatly underestimates the magnitude of the vertical velocity and even results in a different spatial structure because of the frontal meandering. The instantaneous vertical velocity field can look much different than the frontal mean because the time-dependent meandering has associated with it large upwelling and downwelling events (Fig. 7 and S95; Wang 1993; Bower and Rossby 1989). The variance in the vertical velocity is generally several times larger than the frontal mean, as indicated in Fig. 9b by the root-mean-square of the vertical velocity relative to the frontal mean. Thus, while the ageostrophic velocity derived from the two-dimensional model is largely reproduced by the appropriate averaging of the time-dependent front, the variance of the front is large enough to mask this long-term mean in regions where the meander amplitudes are large. The subduction of water from the mixed layer into the stratified interior is thus controlled by the frontal mean ageostrophic circulation cell.

The vertical motions induced by the wave growth along the front also have associated with them a vertical heat flux (conversion of potential energy to kinetic energy). This is compared to the vertical heat flux calculated from the frontal mean ageostrophic circulation in Fig. 10. The total vertical heat flux Q is calculated by integrating over the model domain

$$Q(z) = \frac{1}{\tau}\int_0^\tau \int_{-L/2}^{L/2}\int_{-L/2}^{L/2} \rho c_p (T(x,y,z,t) - T_b(z)) \cdot w(x,y,z,t)\,dx\,dy\,dt, \qquad (8)$$

where $T_b(z)$ is the mean temperature profile. The vertical heat flux due to the frontal mean ageostrophic circulation cell is calculated as

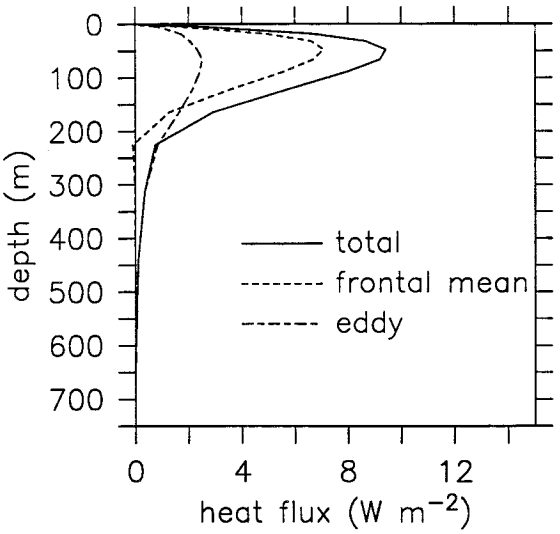

FIG. 10. Vertical heat flux averaged over the horizontal extent of the model domain for the central calculation. The solid line is the total vertical heat flux, the dashed line is the frontal mean vertical heat flux due to the interaction of the large-scale deformation field and the mean baroclinic front, and the mixed-dashed line is the difference, attributed to time-dependent perturbations forced by baroclinic instability.

$$Q_m(z) = \int_{-L/2}^{L/2}\int_{-L/2}^{L/2} \rho c_p(T_m(y', z) - T_b(z)) \cdot w_b(y', z)dx\, dy', \quad (9)$$

where the primes indicate frontal coordinates and the subscript m indicates quantities averaged in frontal coordinates. The difference between $Q(z)$ and $Q_m(z)$ is due to the time-dependent motions that are not represented by a simple meandering of the mean frontal structure, referred to here as the eddy heat flux Q_e. The total vertical heat flux is dominated by the mean ageostrophic vertical circulation cell in the upper ocean, while the smaller eddy heat fluxes are dominant in the deeper ocean. The vertical heat flux is a maximum at approximately 50 m and decays quickly with depth. This result indicates that, while the variability of the vertical velocity is large, the heat flux associated with this variability is much less than the mean vertical heat flux resulting from the essentially two-dimensional interaction between the large-scale deformation field and the relative vorticity in the front. The upwelling and downwelling induced by the frontal meanders is largely occurring along isopycnal surfaces, consistent with the Gulf Stream observations of Bower and Rossby (1989). The positive sign of the eddy heat flux is as expected for baroclinically unstable flows. There is a net vertical heat flux in the statisitical steady state because there is a net heat export through the lateral boundaries at each depth. This vertical heat flux represents a net conversion of potential energy to kinetic energy, and is consistent with the acceleration of the parcels as they are advected into the frontal region.

5. Comparisons with observations

While the present study is process-oriented in nature, there are several robust characteristics of the solutions that warrant some comparison with observations. The FASINEX dataset provides the most detailed oceanic observations of the ageostrophic circulations and surrounding deformation fields available and, in fact, was in large part a motivating factor in the beginning of this study. The general characteristics of the mean baroclinic jet in the central case discussed in sections 2 and 3 compare well with the fronts observed in FASINEX by Eriksen et al. (1991), Pollard and Regier (1992), and H91. The density change across these fronts (0.5 kg m^{-3}), vertical scale of the front (100 m), baroclinic velocity shear (30 cm s^{-1}), and relative vorticities (f/3) all compare well with the fronts in the model.

Estimates of the ageostrophic velocities are somewhat more difficult to obtain from observations. In the vicinity of growing meanders, the deformation field is often enhanced above the large-scale deformation provided by the thermocline eddies by the baroclinic wave (Fig. 7 and S95). Voorhis and Bruce (1982) estimate that, for a large-scale deformation field of strength -10^{-5} s^{-1}, the cross-frontal ageostrophic circulation was 3 cm s^{-1} and the maximum vertical velocity was 30–50 m day^{-1} with downwelling on the cold side of the front and upwelling on the warm side of the front. Pollard and Regier (1992) estimate similar magnitudes and patterns for the ageostrophic circulation in the FASINEX experiment. This compares reasonably well with the ageostrophic velocities found in the vicinity of large amplitude baroclinic waves in section 3. Rudnick (1996) finds cross-frontal velocities of less than 1 cm s^{-1} and vertical velocities of 1 m day^{-1} to 20 m day^{-1} near the Azores Current. Although the horizontal velocity field suggests that there is a large-scale deformation field present, its strength is difficult to estimate reliably from the available data. Nonetheless, the strength and sense of the ageostrophic circulation is consistent with the frontogenesis discussed here.

Rudnick and Weller (1993) found that a residual heat flux of 260 W m^{-2} was required to balance the heat budget at 160-m depth over an area of 2.7×10^8 m^2 in the FASINEX region. They attributed this heating to the ageostrophic vertical circulation cells associated with the FASINEX fronts. If we average this net heat flux over the horizontal area of the present model domain (2.56×10^{10} m^2), this gives a net vertical heat flux of approximately 2.6 W m^{-2}, which compares well with the vertical heat flux estimate at 160 m calculated from the central model calculation in Fig. 10. The magnitude and vertical distribution of the vertical heat flux also compares well with estimates from the Azores Current (Rudnick 1996), which shows a subsurface maximum

of 3–12 W m^{-2} at approximately 150-m depth. The increased depth of the maximum is consistent with the larger vertical scale of the Azores Current compared to the FASINEX fronts.

One robust feature of the FASINEX fronts is that they remain as coherent, identifiable features for periods of up to several months (Voorhis 1969; H91). This is in direct contrast to the spindown via baroclinic instability and eddy formation of FASINEX-like (and other) fronts found in unforced numerical models, that takes place on the order of tens of days (Wang 1993; S95; Samelson and Chapman 1995; Fig. 5a). However, the observations also show that the fronts are highly variable and exhibit periods of meander growth and decay. The present results show that baroclinically unstable fronts that look very much like FASINEX fronts are formed by large-scale deformation fields of strengths typical of the mesoscale eddy field and are maintained for as long as the deformation field persists. If the mesoscale eddy field is modeled as first-mode baroclinic Rossby waves, then this timescale is of the order of 100 days, consistent with the observed persistence of the FASINEX fronts. There is some evidence in satellite sea surface temperature data that the FASINEX fronts may go through periods of relatively large meander amplitudes followed by periods where the fronts are relatively straight (H91), which would be consistent with the vascillation around the mean shear found here, but the data are not sufficient to confirm or reject such a process. Of course, the low-frequency evolution of the deformation field and external surface forcing are not considered here and will probably introduce some further physics into the general problem.

6. Conclusions

The behavior of a baroclinic zone in a barotropic horizontal deformation field has been investigated for both two- and three-dimensional solutions. A major new result reported here is that baroclinic instability can play an important role in limiting the frontogenesis resulting from a large-scale barotropic deformation field. In this time-dependent equilibrated state, large amplitude baroclinic waves flux heat across the front to counteract the convergent heat flux provided by the large-scale deformation. The resulting wave–mean flow interaction leads to a low-frequency oscillation in the strength of the vertical shear and the width of the baroclinic front. Time-dependent equilibrated states are achieved over a wide range of oceanographic and atmospheric regimes spanning the mesoscale to the gyre scale. The model subgrid-scale parameterization limits the frontogenesis in two dimensions, while it remains an important part of the solution in three dimensions.

The ageostrophic circulation in the statistical steady state is that of downwelling on the cold side of the front and upwelling on the warm side of the front with a cross-frontal flow in the upper ocean, in agreement with previous analytic and numerical results. The ageostrophic circulation cell has associated with it a vertical heat flux into the upper ocean that, for parameters typical of open ocean fronts in the North Atlantic subtropical convergence zone (STCZ), is of the same order of magnitude as the annual net surface heat flux into the ocean (5 W m^{-2}) and close to the observational estimates of Rudnick and Weller (1993). Subduction of water from the mixed layer into the stratified interior also occurs at a large-scale average rate of O(10 m yr^{-1}), similar to the annual mean Ekman pumping rate at midlatitudes.

The transition in parameter space from solutions that reproduce the steady two-dimensional result to those that support large amplitude meanders and low-frequency oscillations is understood by making use of Bishop's (1993) time-dependent linear theory to estimate when the nonlinear terms will become important. Strong deformation fields or weak density changes across the front lead to steady, two-dimensional solutions, while weaker deformation fields or stronger density changes result in baroclinic instability and a time-dependent equilibrated state. The frontogenesis provided by the deformation field counteracts the frontolysis of baroclinic instability such that strong [Eady timescale O(1 day)] coherent time-dependent meandering jets are maintained for as long as the deformation field persists. This is in contrast to the rapid breakdown of fronts undergoing baroclinic instability in the absence of any large-scale deformation and may explain the persistence of many open ocean fronts. The suppression of baroclinic instability by the large-scale deformation field suggests that, for strong deformation fields, eddy heat flux parameterizations that are inversely proportional to the Eady timescale (such as proposed by Visbeck et al. 1997) may overestimate the efficiency of frontal mixing by baroclinic instability.

The fronts produced for parameters typical of the North Atlantic STCZ compare reasonably well with various observations. The Rossby number is typically O(0.25–0.5), with maximum alongfront velocities of O(30 cm s^{-1}). While the mean vertical velocity taken in frontal coordinates looks much like the two-dimensional result of O(1 m day^{-1}), for those cases that are unstable, the variability is several times larger so that this mean upwelling and downwelling pattern is not always visible in an instantaneous snapshot of the front. Conversely, the vertical heat flux is dominated by the mean two-dimensional ageostrophic circulation cell, and not by the time-dependent upwelling and downwelling associated with large amplitude meanders. In regions of developing waves, the ageostrophic velocities can be many times larger than the two-dimensional mean as a result of the local enhancement of the deformation field, in general agreement with observations and the previous modeling study of Spall (1995).

Acknowledgments. Support for this work was provided by the Office of Naval Research Grants N00014-90-

J-1490 and N00014-93-1-0572. Helpful comments and suggestions were provided by Prof. Brian Hoskins and an anomymous reviewer.

APPENDIX

The Primitive Equation Model

The numerical model used in this study is based on the Semi-Spectral Primitive Equation Model (SPEM) described by Haidvogel et al. (1991). The version used here uses a finite difference, rather than a spectral, vertical discretization and is described in the SPEM 5.1 User's Guide (K. Hedstrom 1995, personal communication). Although the model formally uses a general stretched coordinate system in the vertical and an orthogonal curvalinear coordinate system in the horizontal, the rectangular domain, flat bottom used here reduces the model to a standard Cartesian coordinate system. For simplicity, the equations are given in this form. The momentum equations are written as

$$\frac{\partial u}{\partial t} + \mathbf{v}\cdot\nabla u - fv = -\frac{\partial \phi}{\partial x} + A_h\nabla^2 u + A_v\frac{\partial^2 u}{\partial z^2} \quad \text{(A1)}$$

$$\frac{\partial v}{\partial t} + \mathbf{v}\cdot\nabla v + fu = -\frac{\partial \phi}{\partial y} + A_h\nabla^2 v + A_v\frac{\partial^2 v}{\partial z^2}, \quad \text{(A2)}$$

where A_h and A_v are horizontal and vertical coefficients of viscosity. The temperature equation, in the absence of external heating, is

$$\frac{\partial T}{\partial t} + \mathbf{v}\cdot\nabla T = K_h\nabla^2 T + K_v\frac{\partial^2 T}{\partial z^2}, \quad \text{(A3)}$$

where K_h and K_v are horizontal and vertical diffusion coefficients. The vertical velocity is calculated from the continuity equation:

$$\frac{\partial u}{\partial x} + \frac{\partial v}{\partial y} + \frac{\partial w}{\partial z} = 0. \quad \text{(A4)}$$

The density is related to the temperature field through a linear equation of state as

$$\rho = 28.0 - 0.14T. \quad \text{(A5)}$$

Finally, the dynamic pressure ϕ is calculated from the density field through the hydrostatic relation

$$\frac{\partial \phi}{\partial z} = \frac{-\rho g}{\rho_0}. \quad \text{(A6)}$$

The surface and bottom boundary conditions are no flux of momentum or heat and zero vertical velocity. The lateral boundary conditions require the specification of the normal and tangential velocities and the temperature. For limited-area calculations such as the present one, this generally requires some form of open boundary conditions. While formally an ill-posed problem, a practical approach has been adopted that seems to behave well for all calculations reported here. On barotropic inflow points, the normal and tangential velocities and the temperature field are held fixed at the same values as in the initial conditions. The northern boundary is a constant source of cold water, while the southern boundary is a constant source of warm water, parameterizing the influences of remote surface forcing, mixed layer physics, and the mesoscale eddy field through the lateral boundary conditions. On barotropic outflow points the transport streamfunction is held fixed at the initial value, while the normal derivatives of the baroclinic velocity components and temperature are taken to be zero. This is equivalent to a one-dimensional radiation condition on these variables with a phase speed equal to $\Delta x/\Delta t$. Sponge layers are introduced within five grid points of the barotropic *inflow* boundaries (northern and southern) such that the baroclinic velocities and the temperature are relaxed toward their specified inflow values with a timescale of 2 days. This was found to suppress Kelvin waves that were generated near the jet outflow points and propagated along the perimeter of the model domain. Analysis of the jet behavior near the boundaries (e.g., Figs. 4, 7) shows no large amplitude influences of the outflow boundary condition on the interior solution, although the vertical velocity can, at times, become large near outflow points. It is likely that such simple boundary conditions perform well here because the persistent outflow supplied by the barotropic flow continually advects these errors out of the model domain.

REFERENCES

Bisagni, J. J., 1991: The relationship of mid-ocean eddy fields to sea surface temperature fronts during the frontal air–sea interaction experiment. Ph.D. thesis, University of Rhode Island, 307 pp.

Bishop, C. H., 1993: On the behavior of baroclinic waves undergoing horizonal deformation. II Error-bound amplification and Rossby wave diagnostics. *Quart. J. Roy. Meteor. Soc.,* **119,** 241–267.

——, and A. J. Thorpe, 1994: Frontal wave stability during moist deformation frontogenesis. Part II: The suppression of nonlinear wave development. *J. Atmos. Sci.,* **51,** 874–888.

Bleck, R., R. Onken, and J. D. Woods, 1988: A two-dimensional model of mesoscale frontogenesis in the ocean. *Quart. J. Roy. Meteor. Soc.,* **114,** 347–371.

Bower, A. S., and T. Rossby, 1989: Evidence of cross-frontal exchange processes in the Gulf Stream based on isopycnal RAFOS float data. *J. Phys. Oceanogr.,* **19,** 1177–1190.

Bretherton, F. P., 1966: Baroclinic instability and the short wave cutoff in terms of potential vorticity. *Quart. J. Roy. Meteor. Soc.,* **92,** 335–345.

Dritchel, D. G., P. H. Haynes, M. N. Juckes, and T. G. Shepard, 1991: The stability of a two-dimensional vorticity filament under uniform strain. *J. Fluid Mech.,* **230,** 647–665.

Eriksen, C. C., R. A. Weller, D. L. Rudnick, R. T. Pollard, and L. A. Regier, 1991: Ocean frontal variability in the Frontal Air–Sea Interaction Experiment. *J. Geophys. Res.,* **96,** 8569–8592.

Flierl, G. R., P. Malanotte-Rizzoli, and N. J. Zabusky, 1987: Nonlinear waves and coherent vortex structures in barotropic jets and β-plane jets. *J. Phys. Oceanogr.,* **17,** 1408–1438.

Gall, R. L., R. T. Williams, and T. L. Clark, 1987: On the minimum scale of surface fronts. *J. Atmos. Sci.,* **44,** 2562–2574.

Hadivogel, D., J. Wilkin, and R. Young, 1991: A semi-spectral primitive equation ocean circulation model using vertical sigma and

orthogonal curvalinear horizontal coordinates. *J. Comput. Phys.*, **94,** 151–184.

Halliwell, G. R., 1997: Sargasso Sea subtropical frontogenesis by synoptic-scale geostrophic flow deformation patterns detected by Geosat altimetry. *J. Phys. Oceanogr.*

——, and P. Cornillon, 1989: Large scale SST anomalies associated with subtropical fronts in the western North Atlantic during FASINEX. *J. Mar. Res.*, **47,** 757–775.

——, ——, K. H. Brink, R. T. Pollard, D. L. Evans, L. A. Regier, J. M. Toole, and R. W. Schmitt, 1991: Descriptive oceanography during the Frontal Air–Sea Interaction Experiment: Medium to large-scale variability. *J. Geophys. Res.*, **96,** 8553–8568.

Holton, J. R., 1979: *An Introduction to Dynamic Meteorology*. Academic Press, 391 pp.

Hoskins, B. J., and F. P. Bretherton, 1972: Atmospheric frontogenesis models: Mathematical formulation and solution. *J. Atmos. Sci.*, **29,** 11–37.

——, and M. A. Pedder, 1980: The diagnosis of middle latitude synoptic development. *Quart. J. Roy. Meteor. Soc.*, **106,** 707–719.

——, M. E. McIntyre, and A. W. Robertson, 1985: On the use and significance of isentropic potential vorticity maps. *Quart. J. Roy. Meteor. Soc.*, **111,** 877–946.

Ikeda, M., and J. R. Apel, 1981: Mesoscale eddies detached from spatially growing meanders in an eastward-flowing oceanic jet using a two-layer quasigeostrophic model. *J. Phys. Oceanogr.* **11,** 1638–1661.

Joly, A., and A. J. Thorpe, 1991: The stability of time-dependent flows: An application to fronts in developing baroclinic waves. *J. Atmos. Sci.*, **48,** 163–182.

MacVean, M. K., and J. D. Woods, 1980: Redistribution of scalars during upper ocean frontogenesis: A numerical model. *Quart. J. Roy. Meteor. Soc.*, **106,** 293–311.

Marshall, J. C., A. J. Nurser, and R. G. Williams, 1993: Inferring the subduction rate and period over the North Atlantic. *J. Phys. Oceanogr.*, **23,** 1315–1329.

Onken, R., 1992: Mesoscale upwelling and density finestructure in the seasonal thermocline—A dynamical model. *J. Phys. Oceanogr.*, **22,** 1257–1273.

Pedlosky, J., 1964: The stability of currents in the atmosphere and ocean: Part I. *J. Atmos. Sci.*, **21,** 201–219.

Pollard, R. T., and L. A. Regier, 1992: Vorticity and vertical circulation at an ocean front. *J. Phys. Oceanogr.*, **22,** 609–625.

Roden, G. I., 1980: On the subtropical frontal zone north of Hawaii during winter. *J. Phys. Oceanogr.*, **10,** 342–362.

Rudnick, D. L., 1996: Intensive surveys of the Azores Front. Part II: Inferring the geostrophic and vertical velocity fields. *J. Geophys. Res.*, **101,** 16 291–16 303.

——, and R. E. Davis, 1988: Frontogenesis in mixed layers. *J. Phys. Oceanogr.* **18,** 434–457.

——, and R. A. Weller, 1993: The heat budget in the North Atlantic subtropical frontal zone. *J. Geophys. Res.*, **98,** 6883–6893.

Samelson, R. M., and D. C. Chapman, 1995: Evolution of the instability of a mixed-layer front. *J. Geophys. Res.*, **100,** 6743–6759.

Sawyer, J. S., 1956: The vertical circulation at meteorological fronts and its relation to frontogenesis. *Proc. Roy. Soc. London*, **A234,** 346–362.

Snyder, C., W. C. Shamarock, and R. Rotunno, 1993: Frontal dynamics near and following frontal collapse. *J. Atmos. Sci.*, **50,** 3194–3211.

Spall, M. A., 1995: Frontogenesis, subduction, and cross-front exchage at upper ocean fronts. *J. Geophys. Res.*, **100,** 2543–2557.

——, and A. R. Robinson, 1990: Regional primitive equation studies of the Gulf Stream meander and ring formation region. *J. Phys. Oceanogr.*, **20,** 985–1016.

Van Woert, M., 1982: The subtropical front: Satellite observations during FRONTS80. *J. Geophys. Res.*, **87,** 9523–9536.

Visbeck, M., J. Marshall, T. Haine, and M. A. Spall, 1997: On the specification of eddy transfer coefficients in coarse resolution ocean circulation models. *J. Phys. Oceanogr.*, **27,** 381–402.

Voorhis, A. D., 1969: The horizontal extent and persistence of thermal fronts in the Sargasso Sea. *Deep-Sea Res.*, **16** (Suppl.), 331–337.

——, and J. G. Bruce, 1982: Small-scale surface stirring and frontogenesis in the subtropical convergence of the western North Atlantic. *J. Mar. Res.*, **40** (Suppl.), 801–821.

Wang, D. P., 1993: Model of frontogenesis: Subduction and upwelling. *J. Mar. Res.*, **51,** 497–513.

Williams, R. T., 1974: Numerical simulation of steady-state fronts. *J. Atmos. Sci.*, **31,** 1286–1296.

Wood, R. A., 1988: Unstable waves on oceanic fronts: Large amplitude behavior and mean flow generation. *J. Phys. Oceanogr.*, **18,** 775–787.